JTTEE5 18:223–230
DOI: 10.1007/s11666-009-9307-4
1059-9630/$19.00 © ASM International

Failure Mechanism for Thermal Fatigue of Thermal Barrier Coating Systems

C. Giolli, A. Scrivani, G. Rizzi, F. Borgioli, G. Bolelli, and L. Lusvarghi

(Submitted August 4, 2008; in revised form January 29, 2009)

Thick thermal barrier coatings (TBCs), consisting of a CoNiCrAlY bond coat and yttria-partially stabilized zirconia top coat with different porosity values, were produced by air plasma spray (APS). The thermal fatigue resistance limit of the TBCs was tested by furnace cycling tests (FCT) according to the specifications of an original equipment manufacturer (OEM). The morphology, residual stresses, and micromechanical properties (microhardness, indentation fracture toughness) of the TBC systems before and after FCT were analyzed. The thermal fatigue resistance increases with the amount of porosity in the top coat. The compressive in-plane stresses increase in the TBC systems after thermal cycling; nevertheless the increasing rate has a trend contrary to the porosity level of top coat. The data suggest that the spallation happens at the TGO/top coat interface. The failure mechanism of thick TBCs was found to be similar to that of conventional thin TBC systems made by APS.

Keywords indentation fracture toughness, instrumented indentation testing, Raman spectroscopy, residual stresses, thermal barrier coatings, thermal fatigue test

1. Introduction

Thermal barrier coatings (TBCs) are applied on gas turbine and aeronautical engine components in order to improve their hot corrosion and oxidation resistances and their service life time through a reduction of the service temperature. The TBC systems consist of a duplex structure made up of a metallic MCrAlY (M stands for either Co, Ni, or Fe or a combination of these elements) bond coat and yttria-partially stabilized zirconia (YPSZ) ceramic top coat (TC). The bond coat is typically deposited by means of either vacuum plasma spray (VPS), air plasma spraying (APS), high-velocity oxy-fuel (HVOF), or chemical vapor deposition (CVD) processes; the YPSZ top coat is typically deposited by an electron beam physical vapor deposition (EB-PVD) process or by an APS process (Ref 1-4).

C. Giolli, Dipartimento di Chimica, Università di Firenze, Via della Lastruccia 3, 50019 Sesto Fiorentino (FI), Italy; **C. Giolli, A. Scrivani,** and **G. Rizzi**, Turbocoating S.p.A., via Mistrali 3, 43010 Rubbiano di Solignano (PR), Italy; **F. Borgioli**, Consorzio Interuniversitario Nazionale per la Scienza e Tecnologia dei Materiali (INSTM), via Benedetto Varchi 59, 50132 Florence, Italy; **F. Borgioli**, Dipartimento di Ingegneria Civile e Ambientale, Università di Firenze, via S. Marta 3, 50139 Florence, Italy; and **G. Bolelli** and **L. Lusvarghi**, Department of Materials and Environmental Engineering, Università degli Studi di Modena e Reggio Emilia, Via Vignolese 905, 41100 Modena (MO), Italy. Contact e-mail: bolelli.giovanni@unimore.it.

Two different kinds of TBC systems exist as a function of their total thickness: thin and thick TBCs. The total thickness is a function of the top coat thickness, which varies according to the application, while the bond coat usually has a thickness between 100 and 200 μm. Thin TBC systems show a total thickness between 300 and 600 μm and the porosity level of the top coat ranges from 5 to 20%. Thick TBC systems can show a total thickness greater than 600 μm up to 2 mm and a porosity level of the top coat up to 30% (Ref 5, 6).

The bond coat surface, onto which the YPSZ-TC is deposited, has a thin oxide layer that mainly consists of various oxides (NiO, $Ni(Cr,Al)_2O_4$, Cr_2O_3, Y_2O_3, Al_2O_3). This thin oxide layer creates the adhesion (bonding) between the metallic bond coat and the ceramic TC (Ref 7). However, during engine operation, another oxide layer forms in addition to the native oxide one. This second layer, which is mainly composed of alumina, is commonly referred to as the ''thermally grown oxide'' (TGO) and it develops slowly during exposure at elevated temperatures (Ref 8-10).

TBC systems have a tendency to fail by spalling or by debonding processes under cyclic high-temperature conditions. TBCs exhibit multiple failure mechanisms. The growth of the TGO between the bond coat and the top coat layers causes large residual stresses, which lead to the spallation of TBC (Ref 11). The situation may be worsened by the formation of spinels, appearing either between the TGO and the bond coat (due to the Al depletion (Ref 12, 13)) or between the TGO and TC (due to the kinetic of the oxidation) (Ref 12, 13): when spinels are formed, it is summarized that their ''brittleness'' results in delamination (Ref 14). The performance of TBCs is also affected by thermal expansion mismatch between the ceramic and the metal, thermal stresses generated by the temperature gradients in the TBC, ceramic sintering, phase transformations, corrosive and erosive attack and residual stresses arising from the deposition process (Ref 15, 16).

The cracking mode is different when YPSZ-TC is produced by either APS or EB-PVD techniques (Ref 17) and it may be influenced also by coating thickness.

Consequently, thick TBCs and traditional thin TBCs cannot be assumed a priori to possess the same failure mechanisms, because of their differences in thickness and microstructure. Normally, the thicker TBCs provide a greater temperature drop across the coatings. In addition, the increased thickness of the coating will increase the stored elastic strain energy and hence the energy release rate for a crack (Ref 18). Thus, the failure mechanisms that cause spallation of thick TBCs might be expected to be different in some degree from those of the traditional thin TBCs. Failure of thin plasma sprayed TBCs occurs in most cases by interface delamination due to different thermomechanical properties of the coating and of the substrate, and to the oxidation of the bond coat (Ref 19-21). In particular, thick TBCs have a worse thermal shock resistance than thin TBCs. Modifications to the microstructure of the YPSZ-TC, as introducing a larger porosity, can increase the thermal shock resistance (Ref 22, 23).

The aim of this work was therefore to study the failure mechanism of thick and porous TBC systems made by APS, under high-temperature thermal fatigue conditions.

2. Experimental

2.1 Samples Preparation

Hastelloy X metal discs (diameter: 25 mm; thickness: 3 mm) were used as substrates for this study. The bond coat of the samples was obtained by means of APS using a commercial CoNiCrAlY powder (chemical composition as AMDRY 995) with a grain size distribution in the range 45-90 μm; the thickness of the bond coat was in the range (250 ± 50) μm. The ceramic TC was subsequently deposited by APS, using an yttria partially stabilized zirconia commercial powder with a grain size distribution in the range of 45-125 μm. The apparent density according to standard ASTM B212 was (2.4 ± 0.1) g/cm^3. Three different sets of spray parameters were employed, in order to produce top coats having different porosity values: these three types of top coats are referred to as Sample 1, Sample 2, and Sample 3, respectively.

2.2 Thermal Fatigue Test

Furnace cycling tests (FCTs) were performed using a test equipment consisting of an isothermal static air furnace (type: 3 zone split tube; maximum temperature: 1300 °C), a specimen tray in Hastelloy X positioned on a vertical elevator, and a circular tube for forced cooling of specimens when the elevator was lowered. Each thermal cycle in the FCT consists of a 5-min heating up to the steady-state temperature, a 45-min soaking at the steady-state temperature of 1150 °C and a 10-min forced air cooling, as shown in Fig. 1. According the original equipment manufacturer (OEM) specifications, the minimum number of thermal cycles requested in order to pass the thermal cycling fatigue test is 250 cycles.

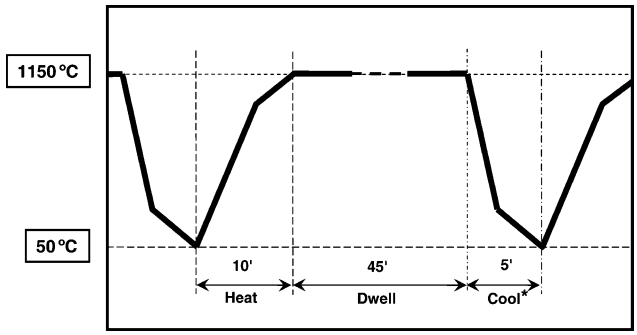

Fig. 1 Time-temperature evolution of one cycle of the furnace cycling test

2.3 Chemical-Physical Characterization

Metallographic investigation was performed using a metallographic optical microscope Zeiss Axiovert 100A with an image analyser based on grey contrast, in order to determine coating microstructure, coating thickness and coating porosity. Specifically, the porosity was measured according to an OEM specification: for each sample, three micrographs (100× magnification) of the polished cross section (vacuum-mounted in epoxy resin) were employed.

Micrographic examination and microprobe analysis were performed by means of environmental scanning electron microscopy (ESEM, QUANTA 200, FEI) with EDAX-ZAF Quantification (Standardless). Raman spectra were recorded using the 514.5 nm line of an Ar^+ laser, a Jobin-Yvon HG2S monochromator equipped with a cooled RCA-C31034A photomultiplier with a 50 mW laser power. The power density measurements were taken with a power meter instrument (model 362; Scientech, Boulder, CO, USA) giving ~5% accuracy in the 300-1000 nm spectral range. X-ray diffraction analysis was performed by using a Philips diffractometer (mod. PW1820) in Bragg-Brentano configuration (Cu Kα radiation generated at 40 kV and 25 mA). Diffraction patterns were analyzed with the MAUD program using the Rietveld method (Ref 24). The residual stresses were evaluated using the $\sin^2 \psi$ method (Ref 25) and additional patterns were collected using a Bruker D8 Advance diffractometer (Cu Kα radiation generated at 40 kV and 30 mA). The ψ angle was changed by rotating the incident angle independently of the detector angle. Patterns in the range $2\theta = 60\text{-}80°$ were collected with different ψ angles in the range −20° to +20° and the residual stresses were measured by evaluating the interplanar spacing variations of the (2 2 0) plane, whose peak was at about $2\theta = 74.2°$. In order to take into account the zero error of ψ, which can be due to both instrumental reasons and sample roughness (Ref 26), the data were fitted as a function of ψ and the zero offset value was determined for each sample.

Microhardness and indentation fracture toughness were measured on the cross sections of the coatings by the Vickers microindentation technique, using a depth-sensing microindenter (Micro-Combi Tester, CSM Instruments,

Peseux, Switzerland), with 2 N indentation load and 1.6 N/min loading/unloading rate. Fifteen indentations were performed on each sample: 5 close to the top surface, 5 in the middle of the coating, and 5 close to the bond coat interface.

Indentation fracture toughness was computed from the length of indentation diagonals and of radial cracks ranging out of the indentation corners, measured using an optical microscope. The Evans-Wilshaw formula (Ref 27), which has already been employed in literature to compute indentation fracture toughness of thermally sprayed coatings (Ref 28-30), was adopted:

$$K_{IC} = 0.079 \frac{P}{a^{3/2}} \log\left(\frac{4.5a}{c}\right)$$

where P is the indentation load (mN), a the indentation half-diagonal (μm), c the average crack length (μm), and K_{IC} is the indentation fracture toughness (MPa*m$^{1/2}$).

3. Results

3.1 Microstructure

Figure 2 shows, as an example, the cross section of one of the thick TBC systems; the bond coat thickness was about 250 μm and the top coat thickness was about 1800 μm for all the sprayed coatings. As shown in a previous paper (Ref 31), three different kinds of samples were obtained as a function of the top coat porosity level measured by image analysis: Sample 1 (TC with 17 ± 1% of porosity), Sample 2 (TC with 21 ± 1% of porosity) and Sample 3 (TC with 29 ± 1% of porosity). X-ray diffraction analysis and Raman spectroscopy showed that the coatings consist essentially of tetragonal zirconia (Ref 31).

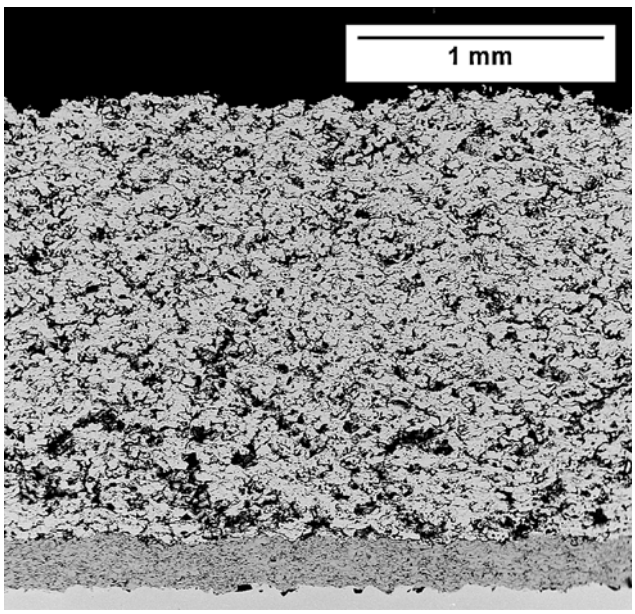

Fig. 2 Backscattered electron scanning electron microscope image of the cross section of a thick TBC system

3.2 Thermal Fatigue Resistance

All the tested samples passed the FCTs according to the OEM specifications (no signs of delamination after 250 cycles). After the thermal cycling test, no detectable change of the phase composition of the top coat was observed, according to x-ray diffraction analysis and Raman spectroscopy as shown in a previous paper (Ref 31).

As 250 FCT cycles were not enough to discriminate between the various coatings, the test was continued up to 455 cycles, in order to achieve a better assessment of the thermal fatigue life. According to the results of these further tests, it could be noted that there is a common trend between the thermal fatigue life time of coated thick TBC and the porosity of YPSZ top coat. Photographs of the thermally cycled TBCs are provided in Fig. 3: for each of the three types of top coats having different porosity (Sample 1, Sample 2, and Sample 3), three specimens are shown (labelled as a, b, and c, respectively). The samples with low porosity (Sample 1) showed the lowest average thermal cycling resistance. The resistance increases in the samples with medium porosity (Sample 2). Among the samples with higher porosity (Sample 3), it is possible to see two samples not damaged and the beginning of spallation in a third one. In all the samples, the first cracking was observed at the extreme edges of the delaminated (Fig. 3, samples 1a and 2a, see arrows) or not delaminated (Fig. 3, samples 1c and 2c, see arrows) samples; cracks then propagated around the sample on further cycling (Fig. 3, sample 3a). It is interesting to note the presence of buckling in the delaminated top coat of sample 1b (Fig. 3, sample 1b, see arrow) and the decohesion of part of the top coat (Fig. 3, sample 3a, see arrow) from the edge and close the edge (Fig. 3, sample 2b). Even in the not delaminated samples (Fig. 4), the crack with larger dimension is localized after 455 cycles at the edge of the sample 3b.

3.3 Bond Coat Behavior

The presence of not damaged samples after 455 cycles was observed for samples with low, medium, and (especially) high top coat porosity level. The bond coat/top coat interface of the Sample 2c after 455 cycles shows the formation of the TGO as shown in Fig. 5. The figure shows that the TGO thickness is not homogeneous and can range from about 5 to 15 μm.

A more detailed SEM image (Fig. 6) of the TGO in the back scattered mode shows that the oxide is formed by two different layers. EDAX data analysis suggests that the outer one (the lighter one) is formed mainly by Cr and O, with minor amounts of Co, Ni, Al, and Y. The inner layer (the darker one) is formed mainly by Cr, Al, and O, with minor amounts of Co, Ni, and Y. The thickness of both layers seems not to be homogeneous; specifically, the thickness of the outer layer grew very inhomogeneously. The same TGO structure and composition were observed in all the analyzed samples after 455 cycles of thermal fatigue test, despite the different top coat porosity levels.

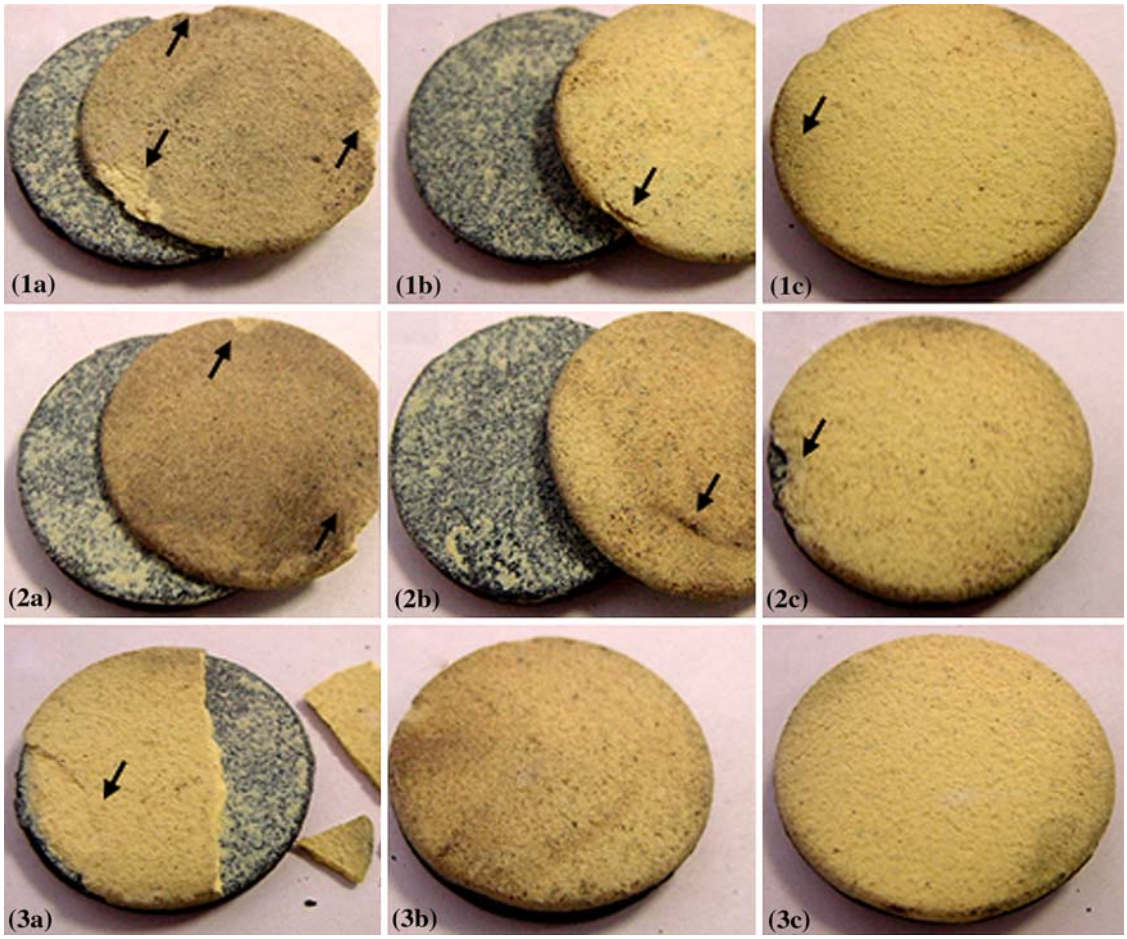

Fig. 3 Photographs of TBCs showing coating failure modes. Sample 1 (17 ± 1% porosity): coatings 1a and 1b delaminated after 305 and 410 cycles at 1150 °C, coating 1c not delaminated after 455 cycles at 1150 °C; Sample 2 (21 ± 1% porosity): coatings 2a and 2b delaminated after 380 and 430 cycles at 1150 °C, coating 2c not delaminated after 455 cycles at 1150 °C; Sample 3 (29 ± 1% porosity): coating 3a, 20% delaminated after 385 cycles at 1150 °C, coatings 3b and 3c not delaminated after 455 cycles at 1150 °C

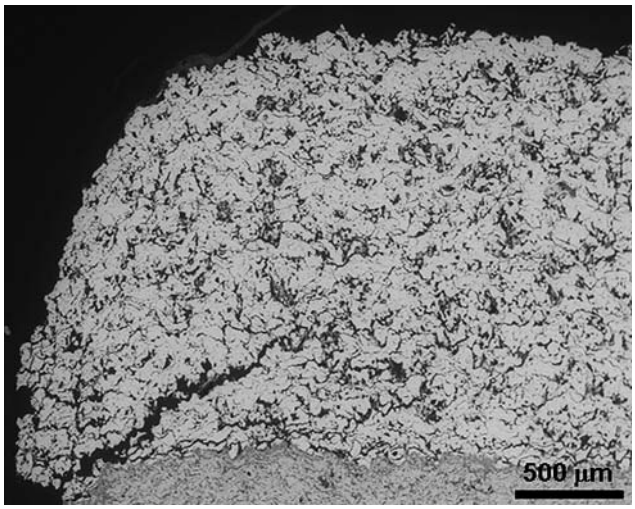

Fig. 4 Initiation of the spallation on the TBC system at the edge of the Sample 3 (29 ± 1% porosity) after 455 cycles

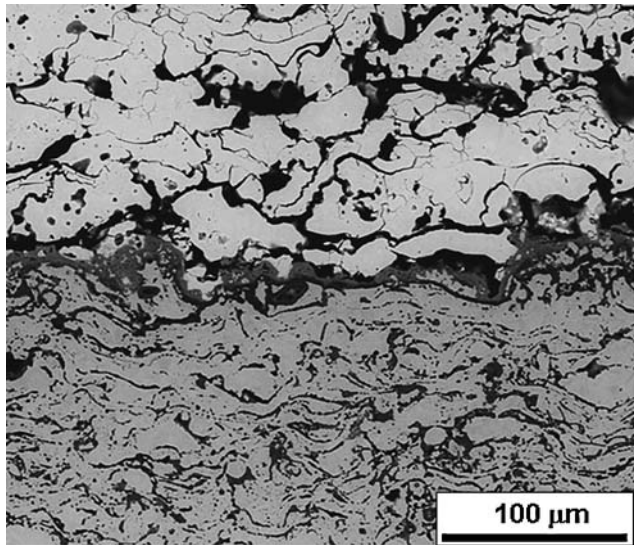

Fig. 5 Bond coat/TGO/top coat interface of Sample 2 after 455 cycles

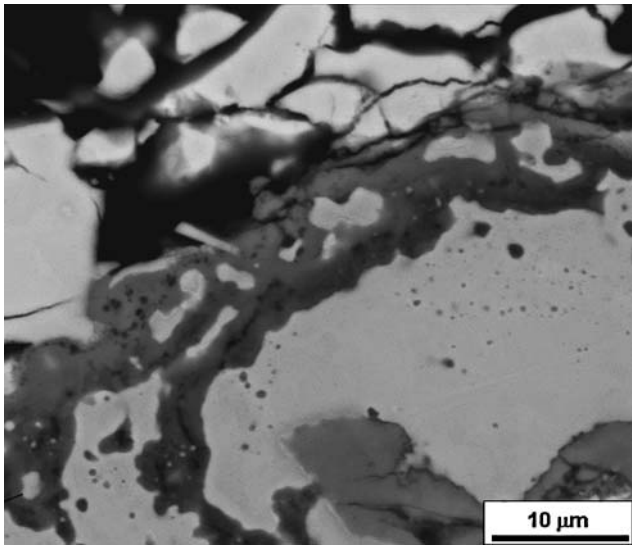

Fig. 6 TGO of Sample 2 after 455 cycles

3.4 Top Coat Behavior

The in-plane residual stresses of the ceramic top coat were evaluated by combining the data obtained by the XRD and the Raman spectroscopy techniques. For each top coat porosity level (Sample 1, Sample 2, and Sample 3), the test was performed both on an as-deposited specimen and on the three specimens (a, b, and c) shown in Fig. 3, subjected to the FCT test.

Residual stresses in the zirconia layer were evaluated before thermal cycling by means of x-ray diffraction analysis using the $\sin^2 \psi$ method (Ref 24, 25), as shown previously (Ref 31). In order to take into account the influence of coating porosity on Young's modulus, the modulus was calculated according to the relationship shown by Kroupa (Ref 32), assuming that crack density is negligible and that, according to the data of Lackey et al. (Ref 17), the Young's modulus of bulk zirconia is 50 GPa and the Poisson's ratio is 0.25.

The residual stress values for the samples are reported in Table 1. For all the samples, compressive stresses are obtained. In the as-deposited condition, the samples with lower porosity (Sample 1) have a significantly higher residual stress value than those with mean (Sample 2) and high (Sample 3) porosity, in accordance with the fact that a higher compliance is expected with higher porosity levels. On the other hand, the samples with medium (2) and high (3) porosity show comparable residual stress values. It has to be pointed out that the obtained residual stress values refer to near-surface regions of the coating, due to the low x-ray penetration in zirconia, and they are typically limited to a depth of about 10 μm or slightly more, depending on the porosity. It may be hypothesized that the absence of a decrease of the residual stress value for Sample 3 in respect to Sample 2 may be due to local strain variations, which affect peak shift, and/or porosity variations and the presence of microcracks, which affect Young's modulus value.

Table 1 Residual stress values of the TBC coatings calculated by the combination of x-ray diffraction and Raman techniques, before (XRD) and after FCT (Raman)

Sample	Porosity, %	Sample state	Residual stress, MPa
1	17 ± 1	As-deposited	−260 ± 30
1a	17 ± 1	Failure after 305 cycles	−546 ± 53
1b	17 ± 1	Failure after 410 cycles	−1448 ± 53
1c	17 ± 1	No failure after 455 cycles	−1602 ± 53
2	21 ± 1	As-deposited	−120 ± 10
2a	21 ± 1	Failure after 380 cycles	−934 ± 45
2b	21 ± 1	Failure after 430 cycles	−1308 ± 45
2c	21 ± 1	No failure after 455 cycles	−714 ± 45
3	29 ± 1	As-deposited	−130 ± 20
3a	29 ± 1	10% of spalling after 385 cycles	−922 ± 48
3b	29 ± 1	No failure after 455 cycles	−592 ± 48
3c	29 ± 1	No failure after 455 cycles	−548 ± 48

For the ZrO_2-8Y_2O_3 plasma sprayed coatings, Teixeira et al. (Ref 33) found a linear relationship between the applied stress and the peak shift of the Raman peaks: each cm^{-1} shift corresponds to a stress of 220 MPa. The accumulated residual stress after thermal cycling was therefore calculated by measuring the Raman shift on samples before and after FCTs and by transforming these peak shift values (expressed in cm^{-1}) to stress changes (expressed in MPa) using the above-mentioned linear relationship (Ref 33), as also explained in Ref 31. The data are summarized in Table 1. The relative errors were calculated by adding the errors of the residual stress measurements before and after FCT. The differences among the Raman peaks before and after FCTs are greater than the evaluated instrumental error that is of the order of ± 0.2 cm^{-1}.

After thermal cycling tests, the compressive in-plane stress always increases in the TBC systems, but the increase becomes less remarkable as the top coat porosity becomes higher (as shown in Fig. 7 as well). The high porosity of the top coat is able to relax the in-plane compressive stresses accumulated during thermal cycling and to increase the resistance of porous thick TBC systems. As shown in a previous paper (Ref 31), it is possible to note that, after thermal cycling tests, the residual stresses seem to be usually lower in the front side of the YPSZ layers than in the back side, suggesting that there is a stress increase at the interface TGO/top coat during thermal fatigue tests where the TBC systems failed.

Sample 1, in as-deposited condition, shows the highest hardness and toughness, whereas the more porous Samples 2 and 3 have significantly lower mechanical properties (Fig. 8 and 9). After thermal cycling, the hardness and fracture toughness of Samples 2 and 3 increase, probably because of the sintering effect during high temperature operation. The first stages of sintering that occurs in TBC top coat are not easily perceivable by means of SEM image analysis, but, in the literature dedicated to this issue, the change in the coating microstructure is usually demonstrated by means of indirect techniques, related to the measurements of the mechanical properties of the as-sprayed and heat-treated top coatings. In particular, the

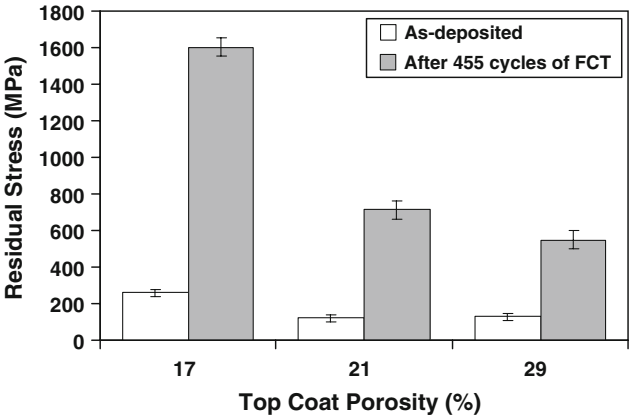

Fig. 7 Absolute value of the residual stresses of the coatings in as-deposited condition and after 455 cycles of FCT. *Note*: all the stresses are compressive

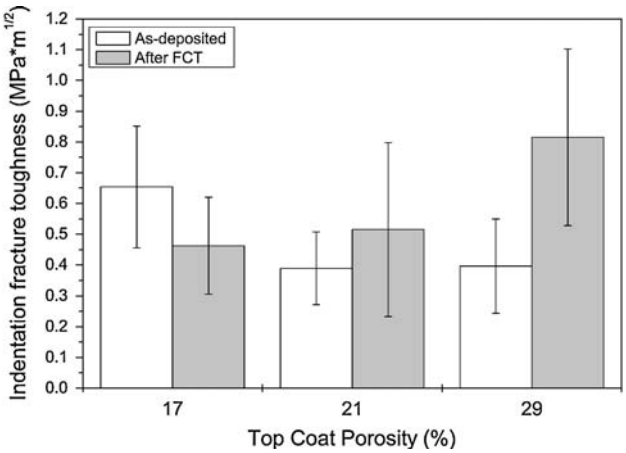

Fig. 8 Indentation fracture toughness of all coatings in as-deposited condition and after FCT (455 cycles)

elastic modulus is often used as crucial parameter to establish the occurring of sintering after isotherm heat treatments of different duration (Ref 34-40). The treatment performed in this study cannot be directly compared to a long isotherm of the same duration, but it consisted anyway of at least more than 300 cycles (300 * 45 min = 225 h). All the abovementioned authors agreed with the fact that this process of sintering/increasing of the mechanical properties occurred very quickly in the first period of the treatment, before reaching a plateau or slowing significantly down. In particular, Guo et al. reported that the elastic modulus has already increased of about 50 GPa in the first 10 h at 1150 °C; Siebert et al. reported that after 2 h the modulus had increased from 94 to 144 GPa at 1100 °C. By contrast, the properties of Sample 1 are degraded and become lower to those of the other thermally cycled coatings. It may be argued that, since the initial as-deposited Sample 1 coating was by far the densest one, the formation of cracks and defects at the interface bond coat/TGO/top coat due to thermal

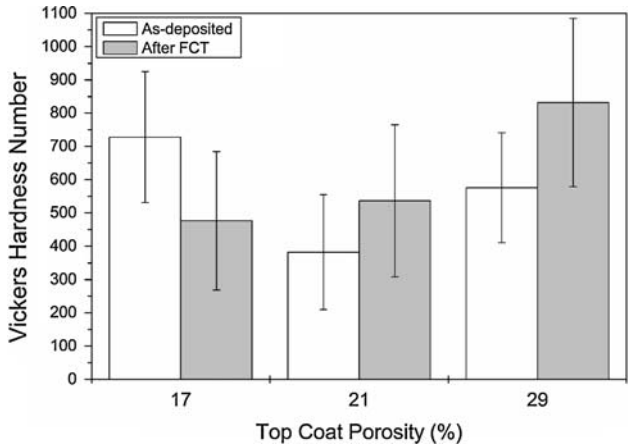

Fig. 9 Vickers microhardness of all coatings in as-deposited condition and after FCT (455 cycles)

shocking is intensified and its negative effect prevails upon sintering effects. The scatter in all measured values (as noted by the standard deviation error bar) is large; indeed, local mechanical properties can vary significantly in highly porous ceramic materials (like TBCs), due to their low Weibull modulus (Ref 41, 42). It is not uncommon to find large scatter in indentation fracture toughness values of thermally sprayed ceramics, but the average K_{IC} value is normally deemed to be significant (Ref 43, 44).

4. Discussion

In general, the spallation process in TBCs is progressive and analogous to the fatigue in metals. The first damages resulted to be localized at the extreme edges of the samples, but they are due to the severe heating and cooling conditions and to stress concentration effects encountered at the edges. For this reason, the edge effect observed in small samples can affect the interpretation of the thermal fatigue failure mechanism of TBC systems (Ref 45). After 455 cycles, the non-delaminated samples show a TGO formed mainly by an outer oxide scale rich in chromium oxides and an inner oxide scale rich in aluminum oxides. Lack of homogeneity in the thickness of TGO is also observed. The presence of local variations in composition and in thickness of TGO may increase residual stress locally and cause the formation of micro-cracks at the interface TGO/top coat. Localized damages could indeed be observed close to the interface TGO/top coat, inside the YPSZ, and rumpling effects are present due to the residual stress accumulated during thermal fatigue tests (Ref 31). Once a single crack gets started, the crack encounters the stress fields; rapid crack link up and macro-crack propagation occurs. Damage progression is often by micro-cracking extension followed by linking-up and then large crack propagation, as observed also previously (Ref 31). All the data suggest that the samples failed close to the interface TGO/top coat. The indentation fracture

toughness of the as-coated samples shows the greatest value for the top coat with low porosity and lower and similar K_{IC} values for the top coat with medium and high porosity level. It is possible to observe the same trend for the residual stresses calculated by XRD technique: the greatest value for the top coat with low porosity and lower and similar σ values for the top coat with medium and high porosity level. Contrarily, after 455 cycles, the top coat having the initially lowest porosity shows the lowest toughness and accumulates the largest compressive residual stress, whereas the top coats having initially higher porosity display increased toughness and lower accumulation of compressive residual stresses. These observations suggest that the denser top coat is severely impaired by thermal cycling; indeed, compressive stresses are built up and, at the same time, thermal shock damage reduces its mechanical properties (hardness, toughness). By contrast, porous top coats undergo less accumulation of compressive stresses and less thermal shock damage: indeed, their mechanical properties, instead of decreasing because of thermal shock damage, are increased by sintering effects.

5. Conclusions

Thick TBC systems, having an average thickness of 1.8 mm and featuring different top coat porosity levels, were made by APS. Thick and porous TBC samples were tested up to their thermal fatigue resistance limits, in order to study their failure mechanisms. The residual stresses and the mechanical properties of the TBC systems were analyzed before and after thermal fatigue tests (FCT) in order to study the failure mechanism. The presence of cracks at the interface TGO/top coat and the rumpling effect are due to the residual stress accumulated during thermal fatigue tests. The presence of TGO imperfections could have increased residual stress locally and caused the formation of micro-cracks at the interface TGO/top coat, as well. The delamination happened when the cracks linked up and macro-crack propagation occurred in presence of the residual stress. Denser top coats are more severely affected by thermal cycling, which is indicated both by the accumulation of very large compressive stresses and by the remarkable decrease in mechanical strength, because of thermal shock damage. Their overall thermal cycling resistance is therefore inferior to that of porous top coats. In the latter, thermal shock damage is much lower; indeed, the effect of top coat sintering on its mechanical properties prevails over the effect of thermal shock damage. Moreover, less build-up of compressive stresses occurs after thermal cycling. Porous top coats are therefore more resistant to thermal cycling than denser ones.

Acknowledgments

This work was partially supported by PRRIITT (Regione Emilia-Romagna, Italy), Net-Lab "Surface and Coatings for Advanced Mechanics and Nanomechanics" (SUP&RMAN).

References

1. W. Brandl, D. Toma, J. Krüger, H.J. Grabke, and G. Matthäus, The Oxidation Behaviour of HVOF Thermal-Sprayed MCrAlY Coatings, *Surf. Coat. Technol.*, 1997, **94-95**, p 21-26
2. D. Toma, W. Brandl, and U. Koster, Studies on the Transient Stage of Oxidation of VPS and HVOF Sprayed MCrAlY Coatings, *Surf. Coat. Technol.*, 1999, **120**, p 8-15
3. E. Lugscheider, C. Herbst, and L. Zhao, Parameter Studies on High-Velocity Oxy-Fuel Spraying of MCrAlY Coatings, *Surf. Coat. Technol.*, 1998, **108-109**(1-3), p 16-23
4. R. Stolle, Conventional and Advanced Coatings for Turbine Airfoils, MTU Aero Engines, D-80995 München. http://www.mtu.de/en/technologies/engineering_news/conventional_and_advanced_coatings.pdf. Accessed May 7
5. J.R. Davis, *Handbook of Thermal Spray Technology*, ASM International, Materials Park, OH, 2005, p 177-178
6. K.E. Schneider, V. Belashchenko, M. Dratwinsky, S. Siegamnn, and A. Zagorski, *Thermal Spraying for Power Generation Components*, Wiley-VCH Verlag GmbH, Weinheim, 2006
7. E.Y. Lee and R.D. Sisson, The Effect of Bond Coat Oxidation on the Failure of Thermal Barrier Coatings, *Thermal Spray Industrial Application*, C.C. Berndt and S. Sampath, Eds., June 20-24, 1994 (Boston, MA), ASM International, 1994, p 55-59
8. Y. Yaslier and S. Alperine, EB-PVD Thermal Barrier Coatings: Comparative Evaluation and Competing Deposition Technologies, AGARD Report 823, Thermal Barrier Coatings, 1998, p 8-10
9. J.A. Haynes, M.K. Ferber, and W.D. Porter, Thermal Cycling Behavior of Plasma-Sprayed Thermal Barrier Coatings with Various MCrAlX Bond Coats, *J. Therm. Spray Technol.*, 2000, **9**(1), p 38-43
10. Y. He, K.N. Lee, S. Tewari, and R.A. Miller, Development of Refractory Silicate-Yttria-Stabilized Zirconia Dual-Layer Thermal Barrier Coatings, *J. Therm. Spray Technol.*, 2000, **9**(1), p 59-64
11. S. Kuroda and T.W. Clyne, The Quenching Stress in Thermally Sprayed Coatings, *Thin Solid Films*, 1991, **200**(1), p 49-66
12. G.C. Wood and F.H. Stott, Oxidation of Alloys, *Mater. Sci. Technol.*, 1987, **3**, p 519-530
13. R. Mevlel, Cyclic Oxidation of High-Temperature Alloys, *Mater. Sci. Technol.*, 1987, **3**, p 531-535
14. A.G. Evans, D.R. Mumm, J.W. Hutchinson, G.H. Meier, and F.S. Pettit, Mechanisms Controlling the Durability of Thermal Barrier Coatings, *Prog. Mater. Sci.*, 2001, **46**(5), p 505-553
15. J. Allen Haynes, E. Douglas Rigney, M.K. Ferber, and W.D. Porter, Thermal Cycling Behavior of Plasma-Sprayed Thermal Barrier Coatings with Various MCrAlY Bond Coats, *J. Therm. Spray Technol.*, 2000, **9**(1), p 38-48
16. P. Scardi, M. Leoni, and L. Bertamini, Influence of Phase Stability on the Residual Stress in Partially Stabilized Zirconia TBC Produced by Plasma Spray, *Surf. Coat. Technol.*, 1995, **76-77**, p 106-112
17. W.J. Lackey, D.P. Stinton, G.A. Cerny, A.C. Schaffhauser, and L.L. Fehrenbacher, Ceramic Coatings for Advanced Heat Engines: A Review and Projection, *Adv. Ceram. Mater.*, 1987, **2**, p 24-30
18. J.W. Hutchinson and Z. Suo, Mixed Mode Cracking in Layered Materials, *Adv. Appl. Mech.*, 1992, **29**, p 63-69
19. E. Tzimas, H. Müllejans, S.D. Peteves, J. Bressers, and W. Stamm, Failure of Thermal Barrier Coating Systems Under Cyclic Thermomechanical Loading, *Acta Mater.*, 2000, **48**(18-19), p 4699-4707
20. G. Qian, T. Nakamura, C.C. Berndt, and S.H. Leigh, Tensile Toughness Test and High Temperature Fracture Analysis of Thermal Barrier Coatings, *Acta Mater.*, 1997, **45**(4), p 1767-1784

21. J.T. De Masi Marcin, K.D. Sheffler, and S. Bose, Mechanisms of Degradation and Failure in a Plasma-Deposited Thermal Barrier Coating, *ASME J. Eng. Gas Turbine Power*, 1990, **112**, p 521-528
22. A. Rabiei and A.G. Evans, Failure Mechanisms Associated with the Thermally Grown Oxide in Plasma-Sprayed Thermal Barrier Coatings, *Acta Mater.*, 2000, **48**(15), p 3963-3976
23. R. Morrell, *Handbook of Properties of Technical and Engineering Ceramics, Part 1*, Her Majesty's Stationery Office, London, 1989
24. L. Lutterotti, S. Matthies, and H.-R. Wenk, MAUD (Material Analysis Using Diffraction): A User Friendly Java Program for Rietveld Texture Analysis and More, *Proceedings of the 12th International Conference on Textures of Materials (ICOTOM-12)*, Vol 1, J.A. Szpunar, Ed. (Ottawa), NRC, 1999, p 1599-1604
25. B.D. Cullity, *Elements of X-ray Diffraction*, Addison-Wesley Publishing, USA, 1978
26. J. Thornton, D. Cookson, and E. Pescott, The Measurement of Strains Within the Bulk of Aged and As-Sprayed Thermal Barrier Coatings Using Synchrotron Radiation, *Surf. Coat. Technol.*, 1999, **120-121**, p 96-102
27. A.F. Evans and T.R. Wilshaw, Quasi-Static Solid Particle Damage in Brittle Solids—I. Observations Analysis and Implications, *Acta Metall.*, 1976, **24**, p 939-956
28. Y. Liu, T.E. Fischer, and A. Dent, Comparison of HVOF and Plasma-Sprayed Alumina-Titania Coatings—Microstructure, Mechanical Properties and Abrasion Behaviour, *Surf. Coat. Technol.*, 2003, **167**(1), p 68-76
29. E. López Cantera and B.G. Mellor, Fracture Toughness and Crack Morphologies in Eroded WC–Co–Cr Thermally Sprayed Coatings, *Mater. Lett.*, 1998, **37**(4-5), p 201-210
30. K.A. Habib, J.J. Saura, C. Ferrer, M.S. Damra, E. Gimenez, and L. Cabedo, Comparison of Flame Sprayed Al_2O_3/TiO_2 Coatings: Their Microstructure, Mechanical Properties and Tribology Behavior, *Surf. Coat. Technol.*, 2006, **201**(3-4), p 1436-1443
31. A. Scrivani, G. Rizzi, U. Bardi, C. Giolli, M. Muniz Miranda, S. Ciattini, A. Fossati, and F. Borgioli, Thermal Fatigue Behavior of Thick and Porous Thermal Barrier Coatings Systems, *J. Therm. Spray Technol.*, 2007, **16**(5-6), p 816-821
32. F. Kroupa, Nonlinear Behaviour in Compression and Tension of Thermally Sprayed Ceramic Coatings, *J. Therm. Spray Technol.*, 2007, **16**(1), p 84-95
33. V. Teixeira, M. Andritschky, W. Fischer, H.P. Buchkremer, and D. Stöver, Analysis of Residual Stresses in Thermal Barrier Coatings, *J. Mater. Process. Technol.*, 1999, **92-93**, p 209-216
34. M. Ahrens, S. Lampenscherf, R. Vaßen, and D. Stöver, Sintering and Creep Processes in Plasma-Sprayed Thermal Barrier Coatings, *J. Therm. Spray Technol.*, 2004, **13**(3), p 432-442
35. J.A. Thompson and T.W. Clyne, The Effect of Heat Treatment on the Stiffness of Zirconia Top Coats in Plasma-Sprayed TBCs, *Acta Mater.*, 2001, **49**, p 1565-1575
36. S.R. Choi, D. Zhu, and R.A. Miller, Effect of Sintering on Mechanical Properties of Plasma-Sprayed Zirconia-Based Thermal Barrier Coatings, *J. Am. Ceram. Soc.*, 2005, **88**(10), p 2859-2867
37. S.A. Tsipas, I.O. Golosnoy, R. Damani, and T.W. Clyne, The Effect of a High Thermal Gradient on Sintering and Stiffening in the Top Coat of a Thermal Barrier Coating System, *J. Therm. Spray Technol.*, 2004, **13**(3), p 370-376
38. F. Cernuschi, P.G. Bison, S. Marinetti, and P. Scardi, Thermophysical, Mechanical and Microstructural Characterization of Aged Free-Standing Plasma-Sprayed Zirconia Coatings, *Acta Mater.*, 2008, **56**, p 4477-4488
39. S. Guo and Y. Kagawa, Young's Moduli of Zirconia Top-Coat and Thermally Grown Oxide in a Plasma-Sprayed Thermal Barrier Coating System, *Scr. Mater.*, 2004, **50**, p 1401-1406
40. B. Siebert, C. Funke, R. Vaßen, and D. Stöver, Changes in Porosity and Young's Modulus Due to Sintering of Plasma Sprayed Thermal Barrier Coatings, *J. Eur. Ceram. Soc.*, 2005, **25**, p 393-400
41. R.S. Lima and B.R. Marple, High Weibull Modulus HVOF Titania Coatings, *J. Therm. Spray Technol.*, 2003, **12**(2), p 240-249
42. S.H. Leigh, C.K. Lin, and C.C. Berndt, Elastic Response of Thermal Spray Deposits Under Indentation Tests, *J. Am. Ceram. Soc.*, 1997, **80**, p 2093-2099
43. M.M. Lima, C. Godoy, P.J. Modenesi, J.C. Avelar-Batista, A. Davison, and A. Matthews, Coating Fracture Toughness Determined by Vickers Indentation: An Important Parameter in Cavitation Erosion Resistance of WC–Co Thermally Sprayed Coatings, *Surf. Coat. Technol.*, 2004, **177-178**, p 489-496
44. R. Venkataraman and R. Krishnamurthy, Evaluation of Fracture Toughness of As Plasma Sprayed Alumina–13 wt.% Titania Coatings by Micro-Indentation Techniques, *J. Eur. Ceram. Soc.*, 2006, **26**, p 3075-3081
45. K. Vaidyanathan, M. Gell, and E. Jordan, Mechanisms of Spallation of Electron Beam Physical Vapor Deposited Thermal Barrier Coatings With and Without Platinum Aluminide Bond Coat Ridges, *Surf. Coat. Technol.*, 2000, **133-134**, p 28-34